An Assessment of the Flux Profile Method for Determining Air–Sea Momentum and Enthalpy Fluxes from Dropsonde Data in Tropical Cyclones

DAVID H. RICHTER AND RACHEL BOHAC

Department of Civil and Environmental Engineering and Earth Sciences, University of Notre Dame, Notre Dame, Indiana

DANIEL P. STERN

University Corporation for Atmospheric Research, Monterey, California

(Manuscript received 2 November 2015, in final form 4 March 2016)

ABSTRACT

An analysis of the reliability of using dropsonde profile data to compute surface flux coefficients of momentum and heat is performed. Monin–Obukhov (MO) similarity theory forms the basis for the flux profile method, where mean profiles of momentum, temperature, and moisture are used to estimate surface fluxes, from which bulk flux coefficients can then be determined given surface conditions. The robustness of this method is studied in terms of its sensitivity to internal, method-based parameters, as well as the uncertainty due to variability in the measurements and errors in the estimates of surface conditions, particularly sea surface temperature. In addition, "virtual sondes" tracked through a high-resolution large-eddy simulation of an idealized tropical cyclone are used to evaluate the flux profile method's ability to recover known surface flux coefficients given known, prescribed surface conditions; this provides a test of whether or not MO assumptions are violated and under which regions they hold. Overall, it is determined that the flux profile method is only accurate within 50% and 200% for the drag coefficient C_D and enthalpy flux coefficient C_K, respectively, and thus is limited in its ability to quantitatively refine model estimates beyond typically used values. Factors such as proximity to the storm center can cause significant errors in both C_D and C_K.

1. Introduction

The specification of bulk flux coefficients in high winds over the ocean has been the subject of much debate in the past two decades. These coefficients, which ultimately determine the surface fluxes of momentum, heat, moisture, and other scalars, are a highly idealized representation of surface transport and are typically cast as functions only of near-surface (typically 10 m) wind speed. At low wind speeds (less than, say, 20 m s^{-1}), the general behavior of these transfer coefficients is well predicted by bulk parameterizations such as the COARE algorithm (Fairall et al. 2003; Edson et al. 2013); in high winds, particularly within tropical cyclones, however, large degrees of observational uncertainty preclude any consensus on their specific behavior. For instance, beginning with the efforts of Powell et al. (2003), it is now generally believed that the drag coefficient C_D either saturates or peaks in high winds, but many details of this saturation process, including the exact "roll off" wind speed or the ultimate physical cause of this plateau, remain unknown. Furthermore, it is becoming increasingly clear that C_D is a function of other factors, particularly wave properties, which can cause modifications of near-surface atmospheric turbulence, leading to a systematic spread in the C_D versus wind speed formulation (Holthuijsen et al. 2012; Takagaki et al. 2012; Reichl et al. 2014; Sullivan and McWilliams 2010).

While many studies attempt to measure the drag coefficient at high winds (Powell et al. 2003; Jarosz et al. 2007; Troitskaya et al. 2012; Vickers et al. 2013; French et al. 2007; Donelan et al. 2004; Potter et al. 2015), far fewer attempt to measure or constrain the thermodynamic flux coefficients. The Humidity Exchange Over

Corresponding author address: David Richter, University of Notre Dame, 156 Fitzpatrick Hall, Notre Dame, IN 46556.
E-mail: david.richter.26@nd.edu

DOI: 10.1175/JAS-D-15-0331.1

the Sea (HEXOS) program (DeCosmo et al. 1996) measured sensible and latent heat fluxes using eddy covariance from a fixed platform in the North Sea and found no statistically significant trend, albeit with expected observational data scatter, of either the sensible heat flux coefficient C_H or the water vapor exchange coefficient C_E with wind speeds up to roughly 20 m s^{-1}. From these measurements they hypothesize that the influence of waves and/or spray is either nonexistent or compensated in some way to yield unchanged flux coefficients.

The high-wind component of the Coupled Boundary Layer Air–Sea Transfer (CBLAST) campaign produced direct, eddy covariance sensible and latent heat flux measurements made from aircraft flown through the boundary layers of Hurricanes Fabian and Isabel in 2003 and found an extended range of insensitivity of C_H and C_E to wind speed out to nearly 30 m s^{-1} (Zhang et al. 2008; Drennan et al. 2007). For these measurements, sea surface temperatures (SSTs) were estimated by a downward-looking infrared radiometer (Black et al. 2007) so that surface temperature and moisture conditions could be used to compute the flux coefficients. By summing the sensible and latent heat fluxes, the total moist enthalpy flux coefficient C_K is also found to remain statistically constant up to 30 m s^{-1} (Zhang et al. 2008). Furthermore, from other components of the CBLAST data (i.e., not just eddy covariance measurements, but including radar, flight-level, and microwave radiometer data as well), Bell et al. (2012) constructed azimuthally averaged energy and angular momentum budgets to estimate the surface fluxes of momentum and enthalpy in regions where direct measurements are unavailable and concluded that C_K, within a large degree of uncertainty, remains in the same range as previous estimates, even beyond wind speeds of 70 m s^{-1}.

In the laboratory, attempts to measure air–sea energy transfer have been performed for many years (Mangarella et al. 1973), but only recently have high-wind conditions been successfully achieved. Haus et al. (2010) and Jeong et al. (2012) used water-side energy budgets to solve for the air–water moist enthalpy flux and found once again that the values of C_K are relatively unchanged up to 10-m wind speeds of roughly 40 m s^{-1}. While the measurement uncertainties of this dataset are much better constrained than the observationally based estimates of C_K, questions remain regarding practical laboratory limitations on factors such as wave age, wave height, spray, and fetch.

The importance of the flux coefficients C_D and C_K, and more generally of the relative balance between energy dissipation through drag and energy input through sensible and latent heat at the air–sea interface, has long been recognized as a key factor for accurately predicting tropical cyclone development and intensity (Rosenthal 1971). The theoretical/numerical work of Emanuel (1986) and Emanuel (1995) predicts that the storm intensity will vary as the square root of the ratio between C_K and C_D, based on axisymmetric thermodynamic budgets of a steady-state system. Other studies have shown the direct, substantial influences of varying surface flux coefficients in numerical predictions of tropical cyclone development, structure, and strength (Montgomery et al. 2010; Bryan 2013, 2012; Green and Zhang 2013; Bao et al. 2011). Generally speaking, increases in C_K lead to overall increases in storm strength, while increases to C_D may nominally decrease storm strength (as defined by the maximum 10-m wind speed), albeit through more complicated alterations to the pressure-gradient wind balance and near-surface inflow. Other studies actually exploit the sensitivity of storm structure to surface flux coefficients to estimate the ''best'' values of C_D or C_K using parameter estimation procedures (Sraj et al. 2013; Green and Zhang 2014; Rios-Berrios et al. 2014).

Meanwhile, it is well recognized that these transfer coefficients are meant to represent myriad small-scale processes in some sort of bulk sense. Therefore many attempts have been made to predict high-wind fluxes of momentum, heat, and moisture based on parameterized considerations of processes such as waves (Kudryavtsev and Makin 2007; Troitskaya et al. 2012; Reichl et al. 2014) or spray (Mueller and Veron 2014; Makin 2005; Fairall et al. 1994; Andreas 2004, 2010; Veron 2015). Unfortunately, however, these often-intricate models are difficult to verify because of the practical difficulties associated with making small-scale, in situ measurements of quantities such as spray generation functions or high-wavenumber surface wave spectra. Moreover, in certain cases, appealingly sound theoretical arguments seem at odds with uncertain measurements, which highlights the need for continuous improvement of both. For instance, surface enthalpy flux models that account for spray, including those of Andreas (2011), Mueller and Veron (2014), and Bao et al. (2011), indicate that C_K may undergo a systematic increase with wind speeds exceeding 30 m s^{-1}, which is seemingly at odds with the observations mentioned above. The observations, however, are highly uncertain at high winds and cannot conclusively rule out the predicted model behavior.

It is this continued limited understanding of air–sea thermodynamic fluxes at high winds that motivates the current work. In a previous study, Richter and Stern (2014) show that mean profiles of temperature and moisture obtained from dropsondes launched within tropical cyclones can be used to construct mean enthalpy profiles that are fitted to estimate surface enthalpy fluxes

[using Monin–Obukhov (MO) similarity theory—herein referred to as the flux profile method]. The work of Richter and Stern (2014) specifically focuses on the evidence of spray-mediated enthalpy fluxes contained within these profiles. Rather than focusing on the behavior of the flux coefficient C_K, power-law scaling exponents of the dimensional enthalpy flux H_K versus wind speed were used to distinguish between laboratory cases, where so-called interfacial fluxes were dominant over spray-mediated enthalpy fluxes and field observations.

The current study aims to quantify the general utility and accuracy of the flux profile method in the context of tropical cyclone winds. The flux profile method is the basis for the study of Powell et al. (2003), which provided the first observational evidence that C_D saturates at high winds. The work of Holthuijsen et al. (2012) is also based on the flux profile method, where the quadrant dependence of C_D was used to infer wave influences on surface momentum fluxes. While each of these studies used profiles obtained from dropsondes, other studies, such as the recent work by Zhao et al. (2015), use multilevel tower data for the same purpose.

Many factors exist, however, that may render inappropriate the use of MO theory (or, equivalently, the existence of a logarithmic surface layer or ''log layer'') in hurricane boundary layers, including, for example, radial pressure balances near the core (Smith and Montgomery 2014). The current work computes dynamic and thermodynamic fluxes and flux coefficients based on mean vertical profiles obtained from dropsondes and discusses the sources of uncertainty and sensitivity in this process. In addition, high-resolution large-eddy simulations, where the turbulent boundary layer is not parameterized, are used to test the ability of emulated dropsonde profiles to recover known surface temperature and flux conditions, thereby assessing the general ability of this method near the core of a simulated tropical cyclone vortex. In general, it appears that the estimates of C_D are accurate within roughly 50%, while estimates of C_K are more subject to uncertainty and are only accurate within roughly 200%.

2. Dropsonde data

a. Method

1) THEORY

To estimate surface fluxes from tropical cyclones, data from GPS dropsondes were obtained from the publicly available datasets provided by the National Oceanic and Atmospheric Administration's (NOAA) Hurricane Research Division (HRD). In total, 2425 dropsonde profiles from 37 different tropical cyclones (ranging in intensity from tropical depression to category-5 hurricane) were used to construct mean profiles of pressure, temperature, humidity, and wind speed. Pressure, temperature, and humidity are measured at a frequency of 2 Hz, as were winds prior to 2010. Starting in 2010, a redesigned sonde was introduced, and winds are now measured at 4 Hz; of the 2425 total sondes, 616 of them were launched in 2010 or later and thus used the redesigned sonde. The sondes are advected horizontally and vertically by the winds, while falling at a density-dependent rate, which is approximately 10–12 m s^{-1} in the lower troposphere. Based on this fall speed, data are sampled every 5–6 m vertically (~3 m for wind speed for the newer sondes). For this dataset, all sondes were dropped by either Air Force C130 or NOAA P3 aircraft, which typically fly at heights of 1.5–4 km. Therefore, the sondes typically take about 3–6 min to fall to the surface. All sondes in this dataset were quality controlled by HRD, using either HRD's Editsonde software or the National Center for Atmospheric Research's Atmospheric Sounding Processing Environment (ASPEN) software. The stated instrumental accuracy of the GPS dropsonde is 0.5 mb (1 mb = 1 hPa), 0.2°C, 2%, and 0.5 m s^{-1} for pressure, temperature, relative humidity, and wind speed, respectively (Hock and Franklin 1999).

The underlying basis of MO theory (see, e.g., Monin and Yaglom 1971) is that mean gradients of velocity or other quantities (referred to here as an arbitrary scalar ϕ) are based solely on the surface flux of that quantity and the height z above the surface (assumed to be much larger than a typical roughness length: $z \gg z_0$). Thus, in regions of the flow without the influence of small-scale surface details, large-scale forcings, or elevated sources or sinks, dimensional analysis predicts that the mean velocity and scalar profiles observe a logarithmic behavior:

$$\langle u \rangle = \frac{u_*}{\kappa} \ln\left(\frac{z}{z_0}\right) \quad \text{and} \tag{1}$$

$$\langle \phi \rangle - \phi_0 = \frac{\phi_*}{\kappa} \ln\left(\frac{z}{z\phi}\right), \tag{2}$$

where it is assumed that the surface conditions are neutrally stable, the surface currents (i.e., the water velocity u_0 at the surface) are negligible,[1] and that the same scaling parameter κ (the von Kármán constant;

[1] If a surface current u_0 was somehow known and not negligible, Eq. (1) could be modified by subtracting u_0 from the left-hand side. Obtaining estimates for surface currents under sonde profiles is, however, nearly impossible, and we assume that the wind speed is everywhere much higher than u_0.

taken to be $\kappa = 0.4$ throughout) is valid for all mean profiles. Note that, by taking $\kappa = 0.4$ for both the velocity and scalar relationships, we have implicitly assumed a turbulent Prandtl number equal to 1; that is, we assume that the turbulent diffusivity of momentum and passive scalars is identical. In general, the value may be slightly less than unity (Monin and Yaglom 1971), but for the present purposes a value of 1 is chosen for simplicity. The averages denoted by $\langle\cdot\rangle$ indicate horizontal or ensemble averages, z_0 is the roughness length, which is defined as the height at which the velocity profile becomes equal to the (negligible) surface current, and z_ϕ is analogously the height where ϕ attains its surface value of ϕ_0.

In Eq. (1), u_* refers to the friction velocity, which is defined based on the total surface stress τ_w:

$$\rho u_*^2 = \tau_w, \tag{3}$$

where ρ is the air density. Likewise, in Eq. (2), ϕ_* is a scale for ϕ determined dimensionally from the surface scalar flux H_ϕ:

$$-\rho u_* \phi_* = H_\phi, \tag{4}$$

where H_ϕ is the upward-directed surface flux of ϕ. It is assumed that the momentum flux τ_w and scalar flux H_ϕ, and thus u_* and ϕ_*, are constant with height given the above conditions. Typically, the constant surface layer fluxes are understood as the turbulent fluxes $\rho\langle u'w'\rangle$ and $\rho\langle w'\phi'\rangle$ in the absence of other mechanisms of vertical momentum or scalar transfer (form stress due to waves, elevated spray sources, etc.), where the primes indicate perturbations from the mean.

Finally, the bulk parameterizations of interest relate the surface fluxes τ_w and H_ϕ to reference conditions, which are often taken as the 10-m mean quantities U_{10} and ϕ_{10}:

$$\tau_w = \rho u_*^2 = \rho C_D U_{10}^2 \quad \text{and} \tag{5}$$

$$H_\phi = -\rho u_* \phi_* = \rho C_\phi U_{10}(\phi_{10} - \phi_0), \tag{6}$$

where C_D is the familiar drag coefficient and C_ϕ is the bulk flux coefficient for the scalar ϕ.

Thus, as long as the aforementioned assumptions hold—namely, negligible surface shape influences (i.e., can be captured solely through a roughness parameterization), no large-scale influences, no elevated sources/sinks, and neutral stability—one can, in theory, obtain the quantities u_* and ϕ_* by determining the slope of $\langle u\rangle$ and $\langle\phi\rangle$ plotted versus the logarithm of z (see Fig. 2). From u_* and ϕ_*, the surface fluxes τ_w and H_ϕ can be readily obtained from the first equality of Eqs. (5) and (6), which, given the surface quantity ϕ_0, can also be used to obtain C_D and C_ϕ via the second equality.

In the present study, the flux coefficients for momentum C_D and enthalpy C_K are of particular interest and will be based on mean profiles of wind speed, potential temperature, specific humidity, and moist enthalpy. Moist enthalpy is defined as the total specific enthalpy of moist air:

$$k = [(1-q)c_{p,a} + qc_l]\theta + L_v q, \tag{7}$$

where $c_{p,a}$ is the specific heat of dry air at constant pressure, c_l is the specific heat of liquid water, θ is the potential temperature, L_v is the latent heat of vaporization, and q is the specific humidity. Note that the potential temperature θ is used in place of true temperature T to eliminate effects of adiabatic expansion with decreasing pressure. In this regard, the reference pressure for converting temperature to potential temperature is the pressure recorded by each individual sonde at the lowest elevation and not the standard reference of 1000 mb.

For determining C_D, the flux profile strategy is relatively straightforward, since surface currents are neglected in comparison to the high-wind speeds. Thus, the value of u_* obtained from the profiles of $\langle u\rangle$ can readily be used to compute C_D, as done in Powell et al. (2003), Holthuijsen et al. (2012), Bi et al. (2015), and Zhao et al. (2015) (again assuming conditions for MO theory hold). For determining the thermodynamic flux coefficients, however, knowledge of SST is required in order to compute the surface conditions of temperature, moisture, and enthalpy [viz., ϕ_0 in Eq. (2)]. Estimates of surface conditions will be discussed in the following section.

2) Adjustable parameters

One of the primary goals of the current study is to assess the accuracy with which the flux profile method can be applied to dropsonde profiles obtained within tropical cyclones, and this requires understanding first how the quantities of interest are sensitive to the parameters of the method. What follows is therefore a description of the procedure for applying the flux profile method to dropsonde data (see Fig. 1 for a schematic).

First, for each sonde, vertically averaged values of the velocity magnitude U_{PBL} [where the subscript refers to planetary boundary layer (PBL)] and enthalpy k_{PBL} are computed by averaging the wind speed and enthalpy profiles below some user-specified height, defined here as H_{mean}. Based on the value of U_{PBL}, the sonde profile is then placed into the appropriate wind speed bin; each has a width $\Delta U_{\mathrm{bin}} = 10\,\mathrm{m\,s^{-1}}$ (the value of ΔU_{bin} does

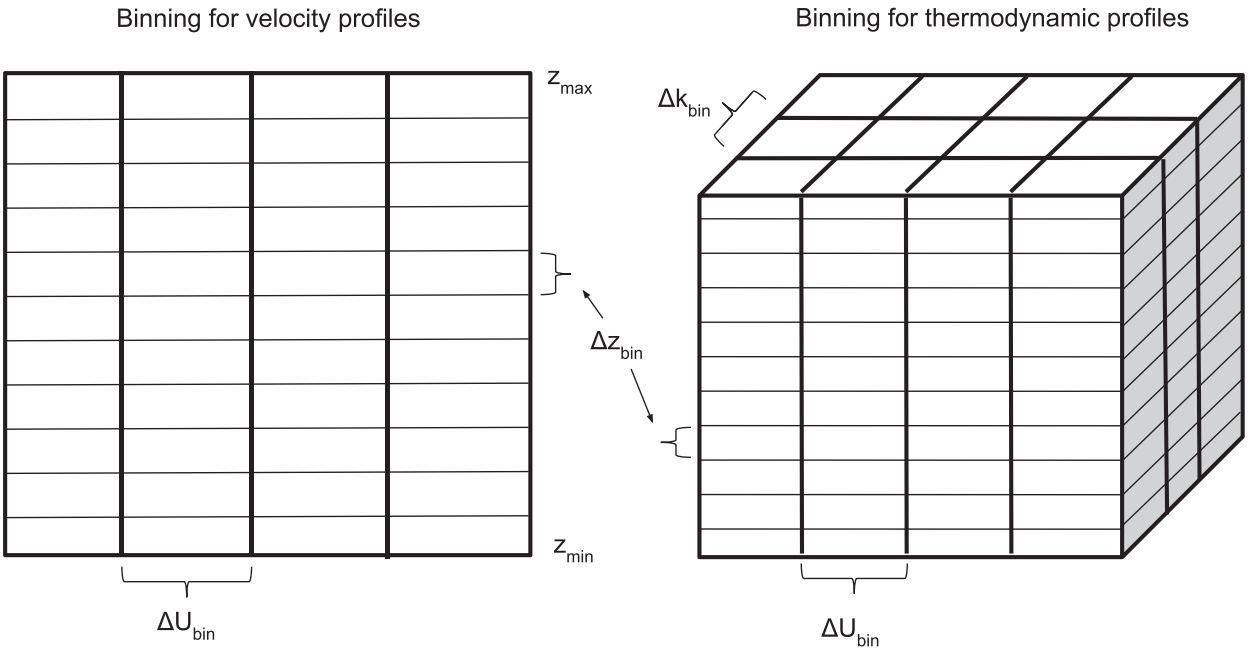

FIG. 1. Schematic of the sonde measurement binning strategy. (left) Each mean velocity profile is binned into a range with width ΔU_{bin} (in this study, $\Delta U_{\text{bin}} = 10\,\text{m s}^{-1}$) based on its value of U_{PBL}, and each individual sonde measurement is binned into vertical ranges Δz_{bin}. (right) Thermodynamic profiles are binned into ranges of both ΔU_{bin} and Δk_{bin} based on values of U_{PBL} and k_{PBL}, respectively, and again each individual sonde measurement is binned into vertical ranges Δz_{bin}.

not change throughout this study)[2]. For purposes of computing surface momentum fluxes and the corresponding values of C_D, no further binning of the sonde is required. For computing surface enthalpy fluxes, however, the thermodynamic profiles (temperature, moisture, enthalpy) are further binned according to k_{PBL} into ranges of Δk_{bin}, the width of which (measured in kilojoules per kilogram) must be chosen.

Once the velocity profiles have been binned according to U_{PBL} and the thermodynamic profiles have been binned according to both U_{PBL} and k_{PBL} (thick lines in Fig. 1), each individual sonde measurement contained in each profile is further binned into uniformly spaced vertical height ranges Δz_{bin} (thin lines in Fig. 1), where the measurements within each height bin are collected and averaged together. Note that the value of Δz_{bin} chosen must be large enough to provide enough samples in each height bin for meaningful statistics but small enough to provide sufficient resolution in the mean vertical profile. What results is a single vertical profile of mean velocity for each wind speed bin and a single mean profile of temperature, moisture, and enthalpy for each combined wind speed and enthalpy bin.

Finally, a choice is made on the height range over which the fit to the mean profiles will be made, which includes specifying a minimum and maximum elevation, denoted z_{min} and z_{max}, respectively. Over this range, a linear regression is then made, where only averages representing the mean of at least 10 data points and regressions over at least 7 vertical points are used. An example is shown in Fig. 2 for a calculation of u_* from mean velocity profiles, where the wind speed bins have a width of $\Delta U_{\text{bin}} = 10\,\text{m s}^{-1}$, $H_{\text{mean}} = 500\,\text{m}$, $z_{\text{min}} = 10\,\text{m}$, $z_{\text{max}} = 100\,\text{m}$, and $\Delta z_{\text{bin}} = 5\,\text{m}$.

Finally, to compute C_K, an estimate is needed of k_0, the surface value of enthalpy, in order to use Eq. (6). This requires knowledge of SST immediately below the mean profiles, which is not recorded by the dropsonde, and therefore an estimate is needed. From the SST, the surface enthalpy is computed by assuming saturation at the SST using the Magnus relation (Dingman 2008):

$$e^* = 6.11 \exp\left(\frac{17.3\text{SST}}{\text{SST} + 237.3}\right), \tag{8}$$

where e^* is the saturation vapor pressure in units of millibars, and SST is provided in degrees Celsius.

As described in Richter and Stern (2014), we use as an estimate for SST the 0.25° Reynolds daily SST analysis (www.ncdc.noaa.gov/cdr/operationalcdrs.html; Reynolds et al. 2007), linearly interpolated to the

[2] For context, Powell et al. (2003) uses $H_{\text{mean}} = 500\,\text{m}$ and $\Delta U_{\text{bin}} = 10\,\text{m s}^{-1}$.

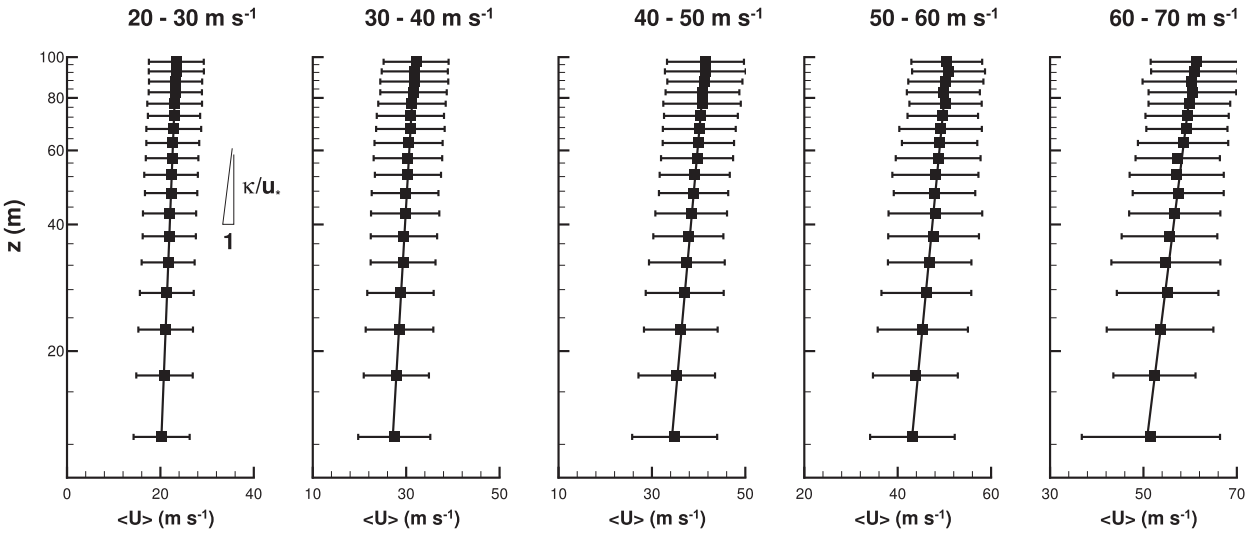

FIG. 2. Semilogarithmic profiles of mean velocity $\langle U \rangle$ with elevation z for wind speed bins of width $\Delta U_{\text{bin}} = 10\,\text{m s}^{-1}$, beginning with $20\,\text{m s}^{-1}$. The horizontal error bars reflect two standard deviations in each direction, and the solid line is a linear regression with a slope of κ/u_*, as noted in the figure. Profiles were created with all 2425 sonde profiles, binning by the mean velocity in the bottom $H_{\text{mean}} = 500\,\text{m}$. (left) The small triangle illustrates the slope of the fitted line.

location of the dropsonde using the nearest analysis in time. Clearly, this method of determining SST immediately below each dropsonde can only be considered a rough estimate. The analysis product is once-daily, so a potentially significant time lag is present for each of the sonde interpolations. Furthermore, this method almost certainly does not adequately capture upper-ocean mixing dynamics, where slow-moving, intense storms upwell cold water to the surface (see, e.g., D'Asaro et al. 2013). In this case, values of SST may be systematically overestimated under certain conditions, which could lead to overestimates of the enthalpy flux coefficient, since large fluxes would be incorrectly associated with small air–sea temperature differences. While the SST estimate is therefore likely a major source of uncertainty (to be evaluated in a later section), it is important to note that this uncertainty only affects the coefficient C_K and not the slope k_* (note that enthalpy k replaces ϕ from the general MO equations of the previous section). By rearranging Eq. (6), it is clear that the uncertainty of SST and therefore C_K is enhanced when k_0 is close in magnitude to k_{10} because the difference appears in the denominator:

$$C_K = \frac{u_* k_*}{U_{10}(k_{10} - k_0)}. \tag{9}$$

Thus, as an additional parameter, we define $\Delta\theta_0 = |\theta_{10} - \text{SST}|$, which is the absolute magnitude of the difference between the 10-m potential temperature and the interpolated value of SST. As done in Richter and Stern (2014) to minimize the impact of the uncertainty of SST, we can exclude sonde profiles with values of $\Delta\theta_0$ under a specified value.

b. Parameter uncertainty

As outlined above, we identify six primary parameters that we are free to choose when extracting momentum and enthalpy flux quantities from dropsonde profiles using the flux profile method: H_{mean}, Δk_{bin}, z_{min}, z_{max}, Δz_{bin}, and $\Delta\theta_0$. The only requirement of these parameters is that they be as consistent with MO theory as possible: that is, quantities such as z_{max} must be within a reasonable range of where one could expect MO theory to hold in the hurricane boundary layer (if it holds at all). Within this broad constraint, the specific values of these parameters are therefore somewhat arbitrary, and for the purposes of this study we choose them to span ranges that are both realistic (e.g., H_{mean} no larger than 500 m, since it is unclear whether or not the boundary layer extends beyond this range) and practical given the available data. As an example, the parameter Δz_{bin} chosen should, in general, be large enough to contain a sufficient number of samples but small enough to provide adequate vertical resolution. While this is nominally straightforward, the dropsondes used for this study were upgraded in 2010, and wind speed collection frequency transitioned from 2 to 4 Hz. Therefore, the choice of Δz_{bin}, while somewhat arbitrary, may potentially influence the mean velocity profiles in nonuniform ways if held constant for all dropsondes. It is this type of influence (as well as that resulting from the other five parameters) that we aim to quantify. We note here that

TABLE 1. Values chosen for each of the six method parameters. Each combination was used to create an ensemble of estimates of u_*, k_*, C_D, and C_K. Bold quantities reflect the baseline case.

Parameter	Values
H_{mean}	100, 250, **500** m
Δk_{bin}	5, **10**, 20 kJ kg^{-1}
z_{min}	**10**, 30 m
z_{max}	**100**, 150 m
Δz_{bin}	2, **5**, 10 m
$\Delta\theta_0$	0, 1, **2** K

the sensitivity to wind speed collection frequency through Δz_{bin} is ultimately found to be minor compared to other sources of uncertainty.

To characterize the robustness of the flux profile procedure, we systematically select the parameters and monitor the variability of the predicted values of u_*, k_*, C_D, and C_K. It is important to note that this test only quantifies the internal sensitivity of this method to the choice of parameters and not the uncertainty due to external influences or measurement error. Before addressing these other sources of error in the following section, it is important to first confirm that the method is reliable in its reproducibility. Table 1 shows the values chosen for each of the six method parameters; each of the $(3)^4 \times (2)^2 = 324$ possible combinations are used to create an ensemble of estimates of the flux quantities u_*, k_*, C_D, and C_K. Again, the values are chosen to span reasonable ranges for each, with the goal of characterizing the sensitivity to freely chosen parameters and bounding the variability in the estimated quantities.

Figure 3 plots the four flux quantities u_*, k_*, C_D, and C_K versus the 10-m wind speed U_{10}, as computed from the linear regression of the mean velocity and enthalpy profiles. In general, Fig. 3 has two features: 1) the retrieved values fall within the range of existing estimates, with the exception of k_* compared to Jeong et al. (2012) [as explained in detail by Richter and Stern (2014)] and 2) the error due to sensitivity of method parameters grows with wind speed, becoming very large at the highest wind speed bin. In Figs. 3a and 3b, the computed values of u_* and C_D, respectively, unsurprisingly lie very close to the observations of Powell et al. (2003) because we use the same method with a moderately expanded dropsonde dataset. The trend of C_D shows a reduction at wind speeds exceeding approximately 35 m s^{-1}, which corresponds to a deviation from linearity of u_* versus U_{10} [cf. Eq. (5)].

Figures 3c and 3d show that, while k_* is relatively well constrained within the same range as the data from Bell et al. (2012) and Zhang et al. (2008), the estimates for C_K show considerable variation as a result of changing the procedural parameters. Even when ignoring the highest wind speed bin, which exhibits an unacceptable variability, sensitivity ranges in C_K at wind speeds exceeding 30 m s^{-1} can approach 200% of the mean predicted value. Ranges of C_D are considerably smaller.

It is therefore instructive to determine which model parameters cause the variability seen in Fig. 3, particularly in the case of C_K. Figure 4 plots the fractions $|C_{D,\text{max}} - C_{D,\text{min}}|/C_D$ and $|C_{K,\text{max}} - C_{K,\text{min}}|/C_K$ versus U_{10}, where subscripts "min" and "max" refer to the minimum and maximum values of C_D and C_K obtained when varying each parameter while holding all others constant at their baseline values (bold quantities in Table 1). Thus, the lines in Fig. 4 show the range of variability as a fraction of the mean flux coefficient due to each of the six parameters (these are not merely the fractional contributions to the total range of Fig. 3; i.e., they do not sum to 1).

Figure 4a shows that the variability in C_D is primarily due to choices of the minimum height z_{min} and the height over which the binning of wind speed is computed H_{mean}. The behavior in Fig. 4a is perhaps unsurprising, given the question of the vertical extent or even the existence of the logarithmic surface layer in the tropical cyclone boundary layer. Note that C_D does not depend at all on Δk_{bin} since velocity profiles are not binned by enthalpy. Furthermore, note that sensitivity to Δz_{bin} is relatively small, which indicates that factors such as the change in wind speed sampling frequency in 2010 (from 2 to 4 Hz) are minor. Figure 4b, on the other hand, shows a scattered response. With the exception of Δk_{bin}, variation in each of the parameters causes significant variation in C_K at some wind speed, although the vertical extent of the enthalpy profiles, given by H_{mean}, z_{min}, and z_{max}, play a very large role at the highest wind speeds. This indicates that the flux profile procedure for obtaining the enthalpy flux coefficient is quite sensitive to the parameters of the method, in particular the specification of the logarithmic layer, and that this sensitivity likely cannot be eliminated by adjustments or improvements to the flux profile procedure. We again emphasize that this only accounts for variability due to method parameters; sensitivity due to external influences will be considered in the following section. Overall, Fig. 4 suggests that in computing either C_D or C_K, specification of the vertical extent of the surface layer is generally the largest source of uncertainty. This sensitivity indicates that external physical processes (i.e., nonsurface-layer processes), such as large-scale pressure gradients or convection, are playing a role and potentially violating the assumptions behind MO similarity. The fact that this sensitivity occurs within $H_{\text{mean}} = 500$ m of the surface furthermore hints at the characteristic height scales at which these external influences become significant factors.

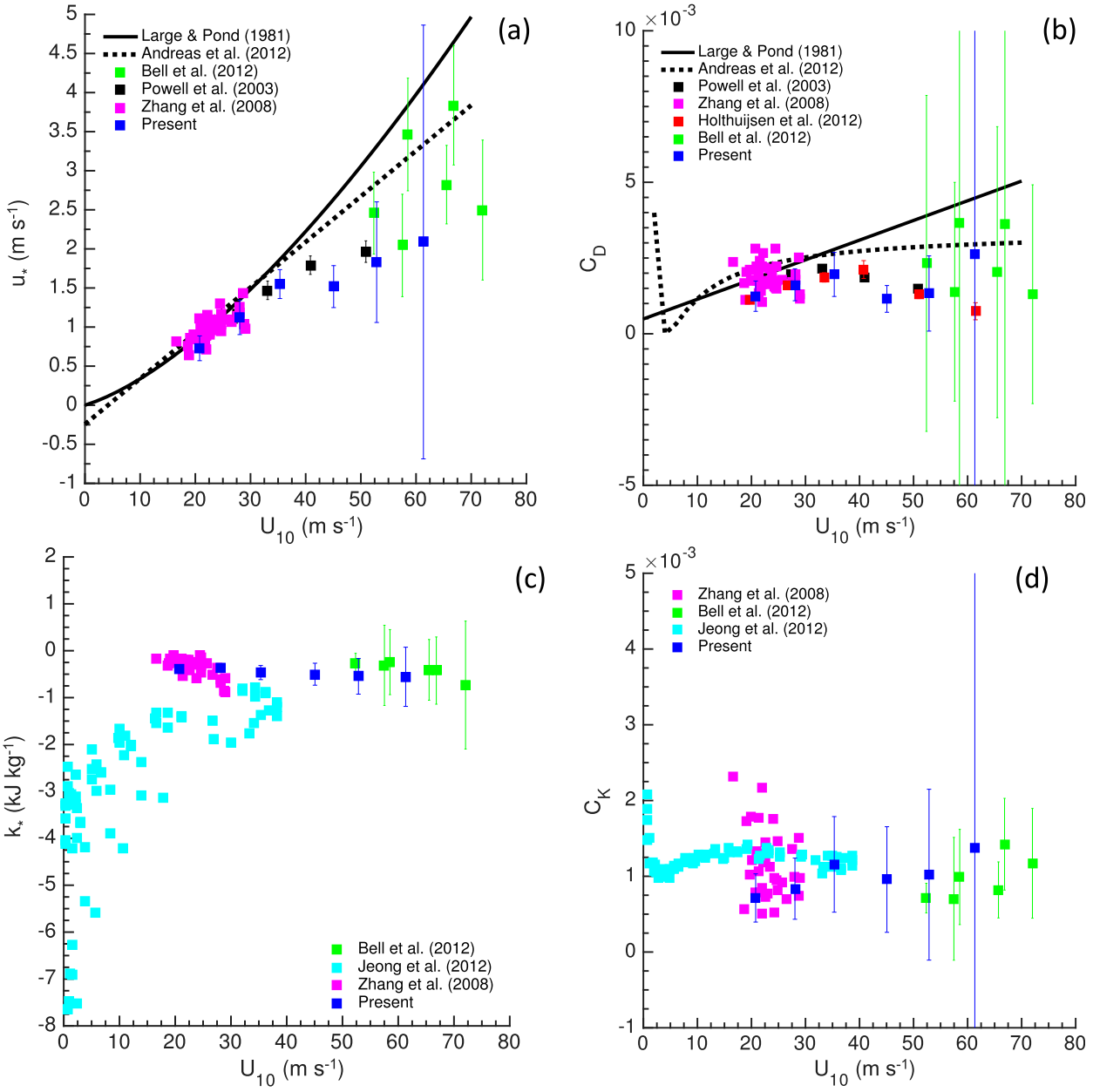

FIG. 3. (a) Friction velocity u_*, (b) drag coefficient C_D, (c) mean enthalpy profile slope k_*, and (d) enthalpy flux coefficient C_K obtained using the flux profile method. The 10-m wind speed determined by the linear regression through the mean velocity and enthalpy profiles is represented by U_{10}. Points and error bars represent the mean and two standard deviations based on the 324-member ensemble with varying combinations of method parameters. Included are existing observational estimates from the literature.

c. *Measurement and SST uncertainty*

Aside from sensitivity to internal parameters of the flux profile method, estimates of C_D and C_K are subject to scatter present in the mean profiles of velocity, moisture, and temperature as well. Furthermore, in the case of enthalpy, the unknown value of SST, which has been interpolated from 0.25° reanalysis data, remains a large source of uncertainty as well. In this section a Monte Carlo–based uncertainty quantification scheme will be used to assess the reliability of the flux coefficient estimates based on the robustness of the logarithmic fit through mean profile data as well as variation in SST.

The horizontal error bars in Fig. 2 illustrate the spread of wind speed data contained within each height and wind speed bin; a similar picture exists for the mean profiles of enthalpy as well (not shown here). Because

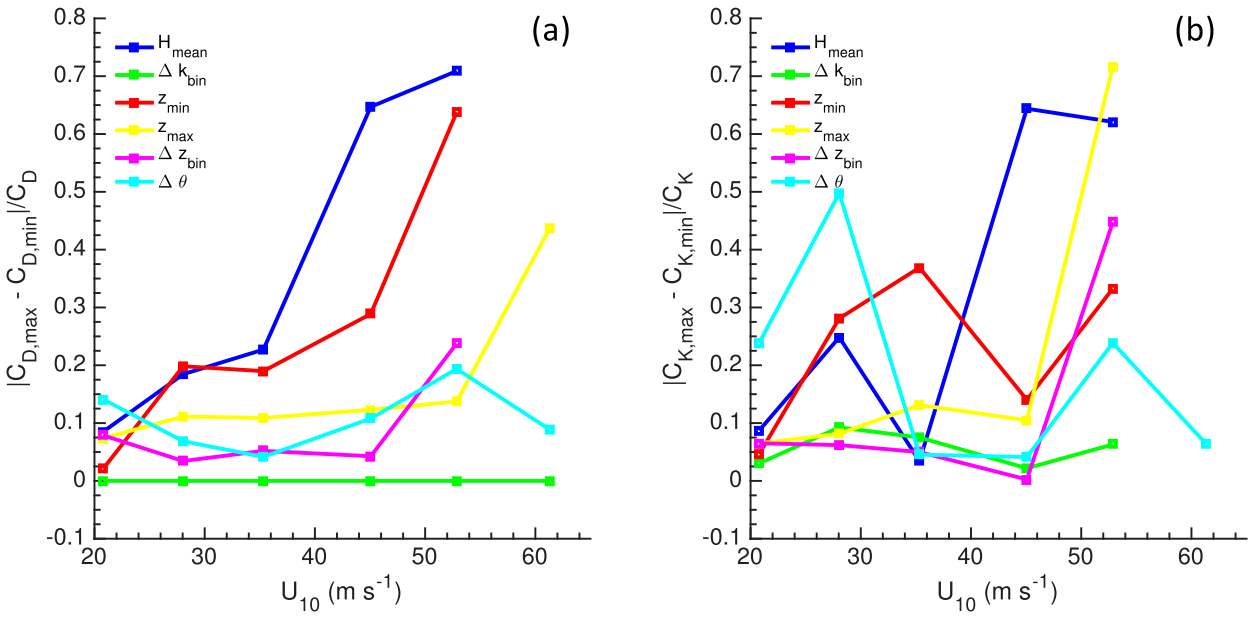

FIG. 4. Plots of (a) $|C_{D,\max} - C_{D,\min}|/C_D$ and (b) $|C_{K,\max} - C_{K,\min}|/C_K$ vs U_{10}, where "max" and "min" refer to the maximum and minimum obtained by varying each of the six parameters outlined in Table 1. See legend for the line associations. Gaps in various curves at the highest wind speed result from a lack of data, where certain combinations of parameters do not meet the criteria for sample size.

the flux profile method depends entirely on the linear regression through the mean values in each height bin, we first consider this regression subject to the 95% confidence interval of each of these mean values. The baseline parameters denoted in boldface in Table 1 are used to perform the binning and fitting procedure.

Because the regression is performed only on the mean values—of which there are only $O(10)$ depending on $z_{\min}$, $z_{\max}$, and Δz_{bin}—and not the "cloud" of all available velocity/enthalpy measurements, standard linear regression errors can be somewhat misleading. For a given wind speed and enthalpy bin (i.e., a single mean profile), we instead use the 95% confidence interval of the mean value in each of the height bins to generate a randomly sampled mean value at each height, where the confidence interval is given by $(\langle x\rangle - 1.96\sigma_x/\sqrt{n_{\text{samp}}}, \langle x\rangle + 1.96\sigma_x/\sqrt{n_{\text{samp}}})$, where $\langle x\rangle$ is the mean value of either wind speed or enthalpy in a particular height bin, σ_x is the standard deviation within that bin, and n_{samp} is the number of samples in that bin. For a Monte Carlo sample size of 10 000, we then assume a normal distribution of the mean value in each height bin with a standard deviation of $1.96\sigma_x/\sqrt{n_{\text{samp}}}$, and compute u_* or k_* (i.e., the slope) as the average of all 10 000 fitted slopes through the profiles of randomly sampled mean values. This is illustrated in Fig. 5, which for a single wind speed and enthalpy bin shows the mean enthalpy points at each height z with their 95% confidence interval, along with 100 of the 10 000 lines fitted through randomly sampled mean values (gray lines). Each of these individual gray lines has its own slope k_*, and the average value across the entire Monte Carlo ensemble results is shown in the solid black line.

Figure 6 shows the values of u_* and k_* as a function of U_{10}, where the error bars now refer to the 10% and 90% quantiles of the 10 000-member ensemble. Compared to Figs. 3a and 3c, the errors associated with the uncertainty of the mean profiles are roughly the same as, perhaps slightly smaller than, the uncertainty associated with the parameters of the flux profile method. Again, the uncertainty increases with increasing wind speed, which results primarily from a decreased number of observational samples and not necessarily a poorer fit. The uncertainty range in Fig. 6 thus illustrates both the spread in available data within each wind speed and enthalpy bin, as well as the robustness of the linear regression. It should be noted that Fig. 6 indicates that MO theory may perhaps hold to an appreciable degree within tropical cyclones in regions where the wind speed is less than roughly 50 m s^{-1}, insofar as the existence of logarithmic mean velocity and enthalpy profiles is proof of this, contrary to Smith and Montgomery (2014). In other words, we would expect the variability in slopes u_* and k_* to be much larger if the mean velocity and enthalpy profiles were not generally logarithmic—a feature suggestive of (but not proof of) the applicability of MO theory.

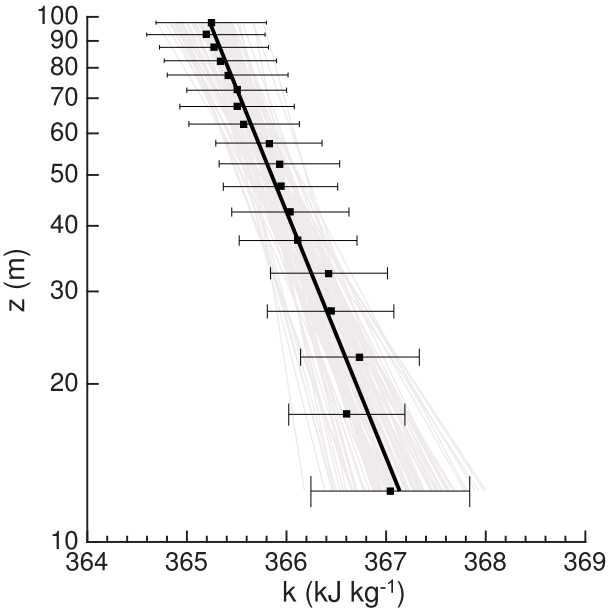

FIG. 5. Sample mean enthalpy profile for the 40–50 m s^{-1} wind speed bin, 350–360 kJ kg^{-1} enthalpy bin. Black symbols represent mean enthalpy with 95% uncertainty range given by error bars. Solid black line represents linear regression through mean enthalpy profile using average value of k_* (over all individual Monte Carlo samples). Gray lines represent 100 of the 10 000 Monte Carlo samples using randomly sampled mean values, given the 95% uncertainty range.

As noted above and in Richter and Stern (2014), u_* and k_* are independent of surface conditions, and thus k_* is not influenced by uncertainty in SST. The flux coefficient C_K, on the other hand, depends heavily on SST through k_0, as shown in Eq. (9). Therefore, for each of the 10 000 Monte Carlo members used to compute the ensemble of mean profile regressions, the value of SST is also sampled from a normal distribution whose mean and standard deviation are equal to the mean and standard deviation of all interpolated values of SST in the corresponding wind speed and enthalpy bin. Note that, because we are using the baseline case, sonde profiles with $\Delta\theta_0 < 2$ K are excluded from this Monte Carlo procedure, and their inclusion in the analysis would only work to increase uncertainty beyond what is reported.

Figure 7 presents C_D and C_K versus U_{10}, where again the symbols refer to the mean of the 10 000-member ensemble and the error bars reflect the 10% and 90% quantile ranges. Included in each panel is a sample probability density function (PDF) from the 40–50 m s^{-1} wind speed, 350–360 kJ kg^{-1} enthalpy bins. The estimates of C_D are not in any way sensitive to SST, and thus their error is only associated with the robustness of the estimate of u_*, as determined by the logarithmic fit. The computed values lie very near those of Powell et al. (2003) and Holthuijsen et al. (2012) because the same procedure is used on nearly the same dataset, but more importantly the uncertainty range is relatively narrow. Aside from the highest wind speed, estimates of C_D obtained from mean velocity profiles appear to be accurate within roughly 50%, taking into account both procedural sensitivity (Fig. 3b) and profile variability (Fig. 7a). The PDF included in the inset shows that the distribution of C_D due to variations of u_* is indeed relatively compact.

Estimates of C_K, however, are again quite uncertain, and the mean computed values are only accurate within roughly 200%. This indicates that, even when excluding sonde profiles where $\Delta\theta_0 < 2$ K, stochastic variability in SST as well as in the mean enthalpy profile leads to relatively large uncertainty in the final value of C_K—an uncertainty on the same order as that resulting from the parameter choices outlined in Table 1. The histogram shown in the inset illustrates the heavy tail that occurs in the PDF of C_K, which is indicative of its larger uncertainty.

Finally, we should note that additional sources of uncertainty exist beyond those induced by procedural parameters, mean profiles, and SST—particularly errors associated with instrumentation. We implicitly assume throughout this analysis that these errors are small compared to those outlined above.

3. Simulation data

As an additional test for determining the reliability of computing C_D and C_K using the flux profile method, we use a high-resolution large-eddy simulation (LES) of an idealized tropical cyclone to construct ''virtual sondes'' that are transported in time and space through the simulated vortex. By taking a large number of virtual sonde profiles and subjecting them to an identical procedure as used for the real dropsonde data, we can compare the computed estimates of C_D and C_K against the surface flux parameterizations that were specified in the LES code. Moreover, a primary benefit of this test is that one of the major sources of uncertainty, SST, is now known exactly. It should be emphasized that this test is meant to further determine the ability of the flux profile method to recover prescribed surface flux parameters from simulated sonde data and not to somehow improve quantitative predictions of C_D or C_K.

We use the Cloud Model 1 (CM1; Bryan and Fritsch 2002; Bryan and Morrison 2012) to simulate an idealized intense tropical cyclone. CM1 is a three-dimensional, nonhydrostatic, fully compressible cloud model that has been used to study a wide range of mesoscale and convective-scale phenomena, including tropical cyclones (e.g., Davis

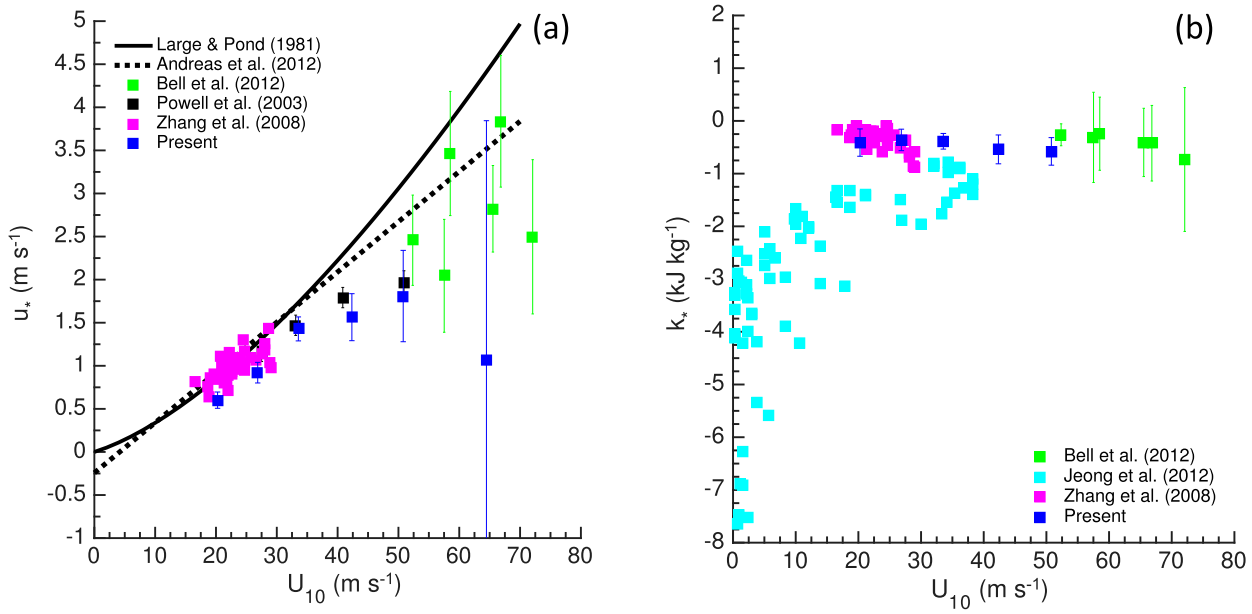

FIG. 6. Plots of (a) u_* and (b) k_* vs U_{10}, where the symbols refer to the average of the 10 000-member Monte Carlo ensemble, where the mean velocity and enthalpy values in each height bin are randomly sampled according to the 95% confidence interval. The error bars refer to the 10% and 90% quantiles of the ensemble.

2015; Bryan and Morrison 2012). CM1 uses a single domain and has grid stretching in both the vertical and horizontal directions in order to maximize resolution in an area of interest while minimizing computational expense. Tropical cyclones are synoptic-scale vortices, so to contain the entire tropical cyclone within our domain, we use a 1486 km × 1486 km grid, with the model top at 25 km. To explicitly resolve most of the large eddies in the boundary layer, we use a horizontal grid spacing of 62.5 m. It is infeasible and unnecessary to use such fine

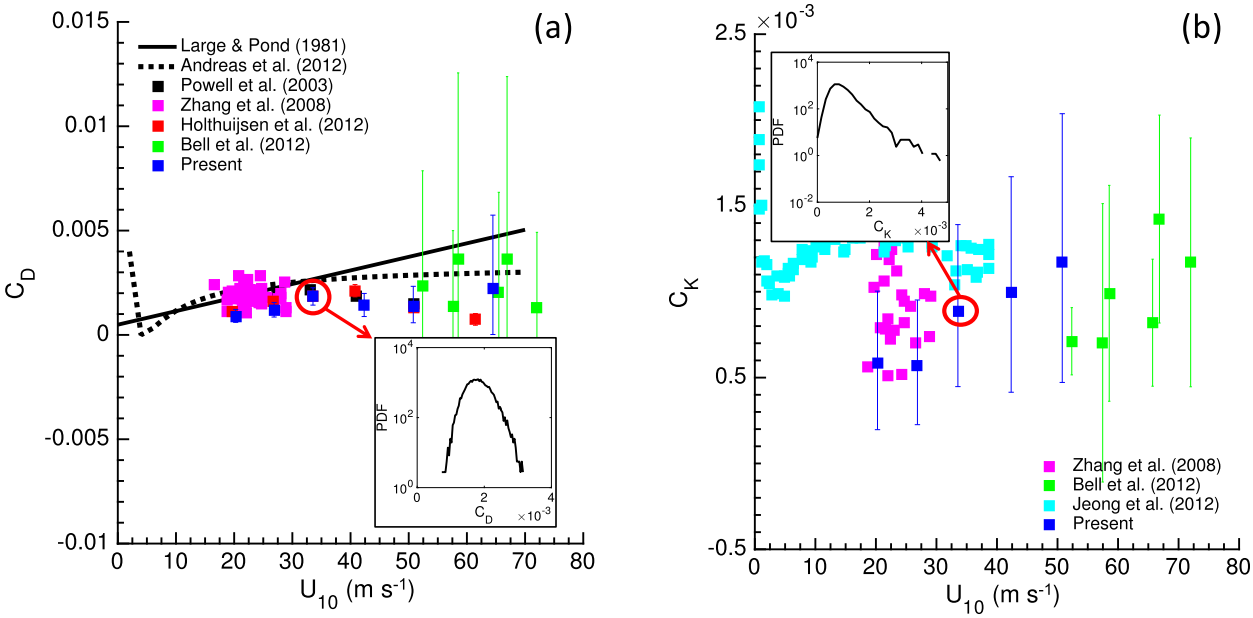

FIG. 7. Plots of (a) C_D and (b) C_K vs U_{10}, where the symbols are the mean of a 10 000-member ensemble, where the SST and the average velocity and enthalpy in each height bin are sampled from normal distributions. The error bars denote the 10% and 90% quantiles of the ensemble. The insets provide probability density functions for representative bins: the 40–50 m s^{-1} wind speed bin and 350–360 kJ kg^{-1} enthalpy bin.

resolution over the entire domain. Our area of interest is the inner-core region, where the eyewall updraft and strongest winds occur; this is also where most of the sondes within our observational dataset are found. Therefore, we use constant 62.5-m horizontal grid spacing in an 80 km × 80 km box centered on the vortex, which is sufficient to cover the entire inner-core region. Outside of this box, the horizontal grid spacing stretches to 15 km by the outer boundary. In the lowest 3 km, vertical grid spacing is constant at 31.25 m (half of the horizontal) and stretches to 500 m near the model top.

We simulate our storm on an f plane, in a quiescent environment (no mean flow), and over a homogeneous and fixed SST of 28°C. The initial atmospheric environment is horizontally homogeneous, using the Dunion (2011) "moist tropical" mean sounding. We insert a balanced, weak vortex into this environment, with initial maximum winds of 20 m s^{-1}. For microphysics, we use the Morrison double-moment scheme (Bryan and Morrison 2012), and we do not parameterize either radiation or convection. Outside of the fine-mesh region, turbulence is entirely unresolved and must be parameterized; for this, we use the turbulence scheme of Bryan and Rotunno (2009). Inside of the fine-mesh region, we turn this parameterization off and only use an LES subgrid model based on that of Deardorff (1980).

Tropical cyclones typically intensify over a period of several days, and even with the grid stretching in CM1, it remains impractical to run our simulation for such a period (there are 1664 × 1664 × 160 grid points). Therefore, we first spin up a tropical cyclone in an axisymmetric version of CM1 and use the time-averaged output from 72 to 84 h, when the tropical cyclone is approximately category 5, to initialize the LES. We then integrate the LES for only 2 h. Though this may seem short, three-dimensional turbulence develops within only 10 min, and the turbulence is statistically steady after an hour (not shown). In a future publication, we will present this and other such simulations in much greater detail.

To emulate dropsondes within the simulation, we calculate parcel trajectories that we modify by adding a fall speed. We use the exact same density-dependent fall speed formulation that is used in ASPEN for the observed sondes. These virtual dropsonde trajectories are integrated within the model using a second-order Runge–Kutta scheme. For the results presented below, we released sondes in a 20 km × 20 km box that covers the southwest quadrant of the simulated tropical cyclone (TC). Sondes are placed at 62.5-m intervals horizontally (i.e., at every model grid point), and in total there are 103 041 virtual sondes. The initial height of all sondes is 2500 m, which is a typical release height for observed sondes. Recall that the observed sondes sample two or four times per second; in order to minimize storage space, we output virtual sonde data only every 3 s. As each virtual sonde samples slightly different heights because of differences in vertical velocities (of the air) and as we are bin averaging the profiles, this difference in sampling rate between the observed and virtual sondes should not substantially affect our results. The sondes are all released at $t = 2$ h, and their trajectories are integrated for 10 min, which is enough time for almost all of the sondes to fall to the surface.

TABLE 2. Values chosen for each of the method parameters for the virtual sonde experiments. Each combination was used to create an ensemble of estimates of C_D and C_K.

Parameter	Values
H_{mean}	100, 250, 500 m
Δk_{bin}	2, 5, 10 kJ kg^{-1}
z_{min}	20, 50 m
z_{max}	100, 150 m
Δz_{bin}	2, 5, 10 m

For estimating C_D and C_K from the virtual sonde profiles, the exact same procedure outlined in section 2a is used, but now the parameter $\Delta\theta_0$ is not needed because there is only a single known value of SST. Once again the reliability of this method is evaluated based on the sensitivity of C_D and C_K to method parameters. Table 2 is analogous to Table 1 and shows the values chosen for H_{mean}, Δk_{bin}, z_{min}, z_{max}, and Δz_{bin} used in the virtual sonde analysis. Note that z_{min} and Δk_{bin} both deviate slightly from the previous case because of restrictions of the computational grid and choice of boundary conditions, respectively.

Figure 8 shows C_D and C_K computed from the 103 041 virtual sonde profiles from a single storm using the flux profile method. As with the real sondes, internal variability of C_K due to method parameters is much larger than that associated with C_D. Predictions of both C_D and C_K lie in the general proximity of the prescribed values (given by the solid blue lines), particularly at the highest wind speeds. Between wind speeds of 20 and 40 m s^{-1}, however, both C_D and C_K underpredict the true value by over 100% (i.e., by a factor of 2).

While this test is of course limited by the accuracy of the turbulence generated by the simulation, it once again confirms that the flux profile method is able to provide estimates of flux coefficients that lie in the correct general range but that are limited in their quantitative calculation. It is worthwhile to caution that purely numerical aspects, such as the vertical grid resolution and details of the LES subgrid model, can and do influence the calculation of C_D and C_K using the virtual sonde approach (not shown). While these factors are unavoidable, we argue that they are small enough that valuable insight can be gained into the validity and robustness of the flux profile method.

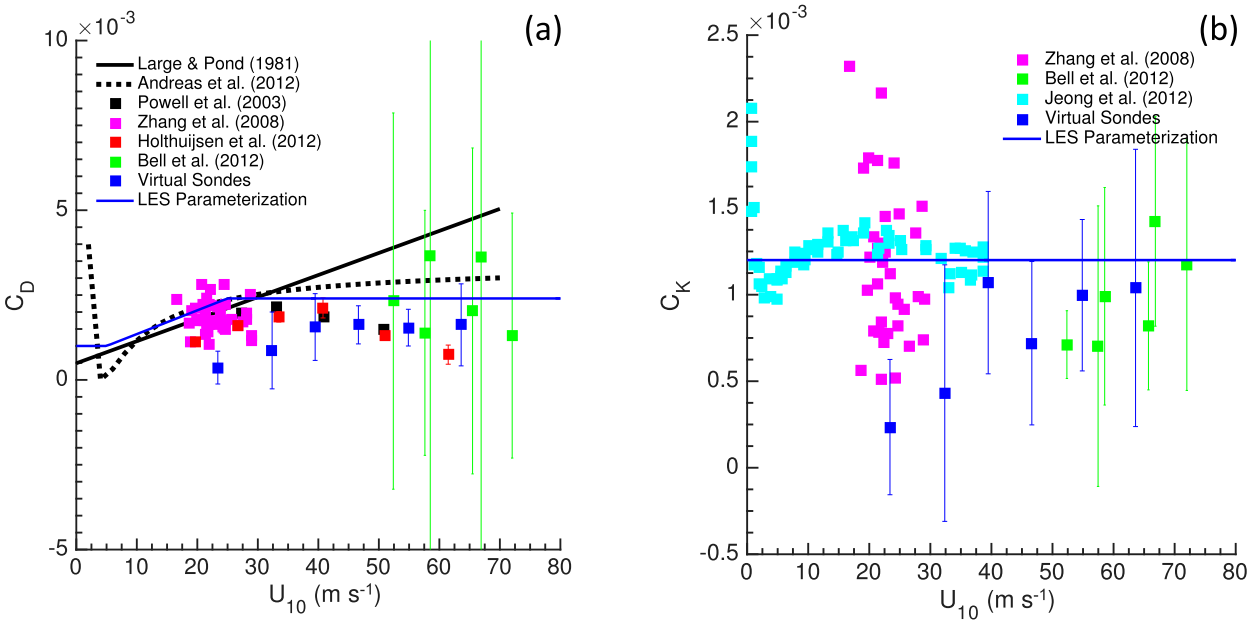

FIG. 8. Plots of (a) C_D and (b) C_K vs U_{10} as estimated from the virtual sonde data. The solid blue lines correspond to the prescribed surface flux coefficients in the code. The error bars reflect two standard deviations from the mean of the $(3)^3 \times (2)^2 = 108$-member ensemble based on the combinations of parameters in Table 2.

4. Discussion

Given the above results for both the real and simulated sonde profiles, two specific points merit further discussion. The first is regarding the agreement (or lack thereof) between the virtual sonde predictions of the surface flux coefficients and the prescribed values shown in Fig. 8. The other is regarding the relationship between C_K and its sensible and latent heat counterparts C_H and C_E, since these are typically the values of practical interest in numerical weather prediction models.

a. Radius dependence

In section 3, virtual sonde trajectories in a turbulence-resolving LES were used to test the flux profile method under conditions where both the SST and the actual surface flux parameterizations are known exactly. Figure 8 indicated that the mean values obtained by the flux profile method agreed qualitatively with real sonde data but underestimated the prescribed values somewhat, particularly at lower wind speeds.

Under conditions where the mean profiles of various quantities are not determined exclusively by the surface flux and the height above the surface (i.e., the underlying basis of MO theory), the existence of a logarithmic layer may be called into question, particularly one that extends an appreciable distance upward from the ocean surface. One such violation is discussed in detail by Smith and Montgomery (2014), who argue that radial pressure balances near the eye of the tropical cyclone violate the underlying assumptions behind the existence of a logarithmic velocity profile.

We therefore perform a simple test to determine what, if any, sensitivity the flux profile predictions of C_D and C_K have to r_{sonde}, the distance from the simulated storm center at which the virtual sonde is released. In Fig. 9, two curves of C_D and C_K are provided: one using sondes in the range $0 < r_{\text{sonde}} < 10$ km and the other only using sondes in the range $10 < r_{\text{sonde}} < 20$ km. For this simulated storm, the radius of maximum wind near the surface is approximately 12 km.

It is clear from Fig. 9 that proximity to the storm center indeed significantly changes the prediction of the surface flux coefficients via the flux profile method. For the range $0 < r_{\text{sonde}} < 10$ km, both C_D and C_K severely underpredict the prescribed values, while for the range $10 < r_{\text{sonde}} < 20$ km the estimated mean values are in close agreement with the prescribed values. In this case, however (Figs. 9c,d), a large degree of uncertainty continues to exist, particularly for C_K, as given by the variability resulting from changing the parameters of the method (see discussion in section 3).

Figure 9 would therefore suggest that the flux profile method is inappropriate in regions near the tropical cyclone eye and could possibly lead to underpredictions of C_D and C_K if these sonde profiles are included in the flux profile analysis, perhaps for reasons given by Smith and Montgomery (2014). Another possibility is that we

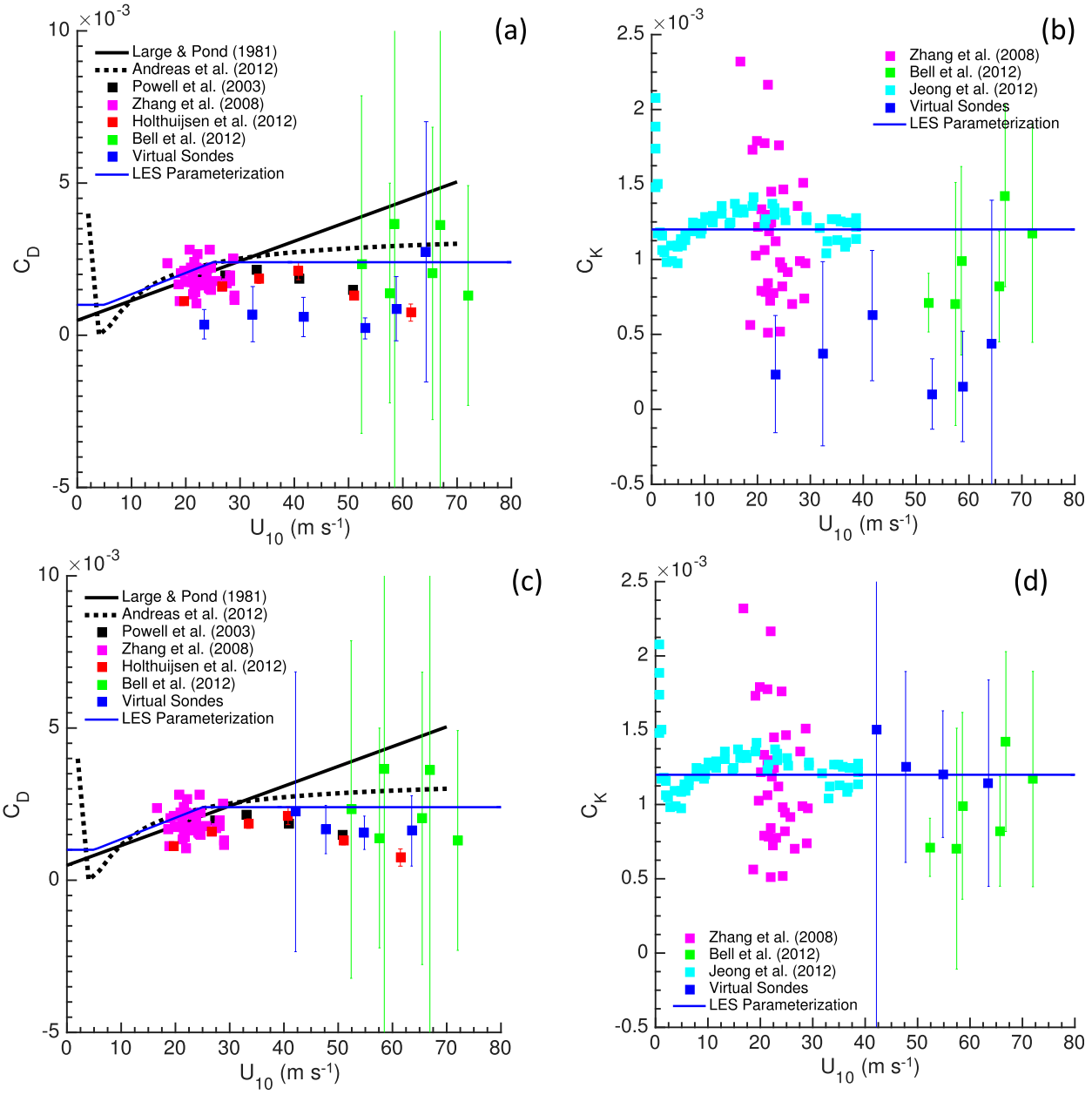

FIG. 9. Plots of (a) C_D and (b) C_K vs U_{10}, as estimated from the virtual sonde data, using only sondes launched in the range $0 < r_{\text{sonde}} < 10$ km. (c),(d) As in (a),(b), but using only sondes launched in the range $10 < r_{\text{sonde}} < 20$ km.

have assumed neutral stability throughout our analysis, which may corrupt the use of the flux profile method in regions near the storm center that are nearly completely dominated by convection. Finally, we note that we have chosen not to restrict the actual sonde data of section 2 in a similar way because of the large degree of uncertainty associated with the storm center and radius of maximum wind at the time of each individual dropsonde launch. We fear that incompatible sonde exclusions would be made between storms of varying size without reliable, time-resolved information regarding the storm center and radius of maximum wind.

b. *Sensible and latent heat fluxes*

A common assumption in boundary layer flux parameterizations is that the flux coefficients for sensible heat, moisture, and enthalpy are the same; that is, $C_H = C_E = C_K$, where Eq. (6) is invoked using $\phi = c_{p,a}\theta, q$, and k, respectively. Past studies that compute fluxes directly (i.e., using eddy covariance) have shown that, within

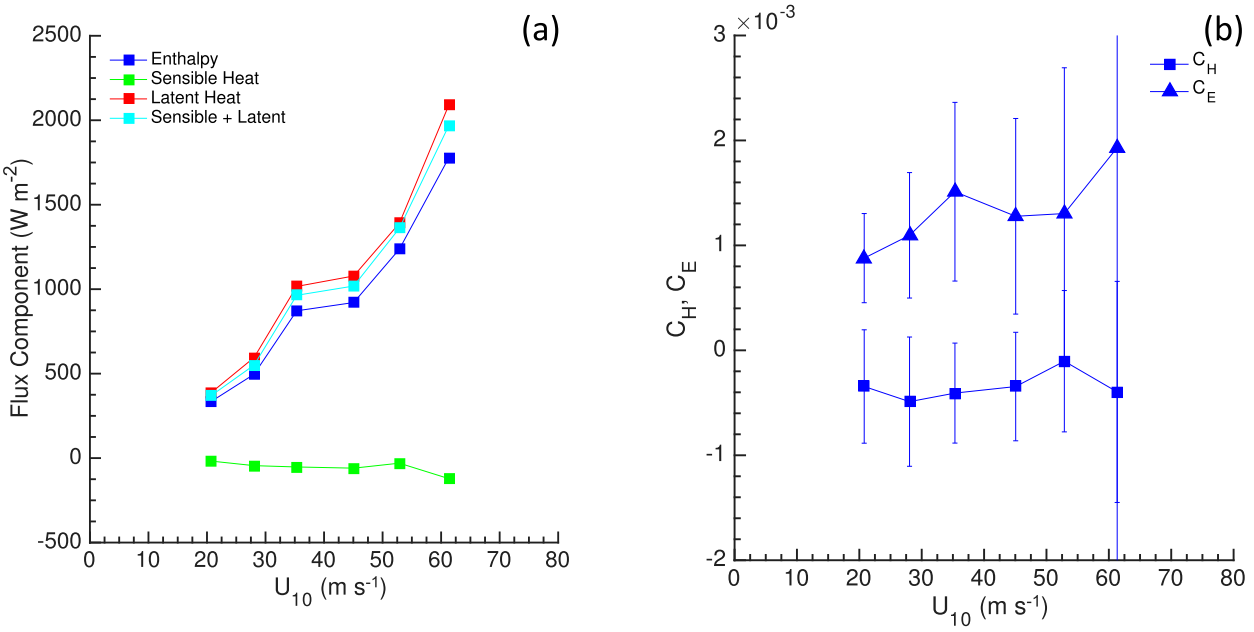

FIG. 10. (a) The fluxes of enthalpy, sensible heat, and latent heat as computed by Eq. (6). The sum of the latent and sensible heat is shown as well, which should ideally match the enthalpy flux as computed via k_* and u_*, given perfect adherence to MO theory. (b) The sensible heat and water vapor flux coefficients C_H and C_E, respectively, as a function of U_{10}.

uncertainty, this relationship holds true (DeCosmo et al. 1996; Drennan et al. 2007; Zhang et al. 2008). In the current context, we noted above that one of the requirements of MO theory is that there exist no elevated sources of the quantity of interest, including those due to evaporation/condensation. Thus, instead of computing fluxes of heat and moisture separately (which are potentially influenced by evaporation and condensation of rain and/or spray), we have focused so far primarily on the flux of moist enthalpy k, since it is conserved during phase transitions and therefore does not violate this MO criterion.

It is worthwhile to comment, however, on the predictions of latent and sensible heat flux as computed by the flux profile method using the observational (i.e., not the virtual) dropsonde dataset. The procedure outlined in section 2 can be used on mean profiles of temperature and moisture, in conjunction with Eq. (6), to compute estimates of surface fluxes of sensible and latent heat over all 37 tropical cyclones:

$$H_S = -\rho c_{p,a} u_* \theta_* \tag{10}$$

and

$$H_L = -\rho(L_v + c_{p,l}\theta_{\mathrm{SST}}) u_* q_*, \tag{11}$$

respectively, where θ_* and q_* are computed via the slopes of the mean temperature and moisture profiles, and θ_{SST} is a mean SST, which we have crudely estimated to be 300 K (this term is overwhelmed by the latent heat of vaporization).

Figure 10a shows H_S and H_L as a function of U_{10}, along with the enthalpy flux as computed by $H_K = -\rho u_* k_*$ for the real sonde data. Also shown is the sum of H_S and H_L, which should ideally sum to exactly H_K. Discrepancies between H_K and $H_S + H_L$ are likely due to violations of MO assumptions induced by evaporating/condensing rainfall or spray within the lower boundary layer, thus making neither temperature nor moisture a conserved quantity. Figure 10a shows a close agreement between the two, suggesting that nonconservative effects may be small. Figure 10a illustrates that latent heat overwhelmingly dominates the total enthalpy flux, somewhat unsurprisingly, and that the sensible heat flux, as computed by this method, is slightly negative.

If the flux coefficients C_H and C_E are computed, however, (Fig. 10b), the values of C_H are actually negative, suggesting that sensible heat is being transported countergradient according to Eq. (6). This is likely unphysical and results from a combination of small-in-magnitude sensible heat fluxes and highly uncertain values of SST. The values of C_E, on the other hand, are quite similar to the values of C_K. Therefore, in this case, the relationship $C_E = C_K$ seems plausible (within uncertainty) but cannot be confirmed or refuted for C_H

because of what is essentially a large signal-to-noise ratio of sensible heat flux to unknown SST values.

5. Conclusions

Dropsonde data recorded across 37 different tropical cyclones were used to construct mean profiles of wind speed and enthalpy in order to use MO theory and the flux profile method to estimate surface fluxes and surface flux coefficients. Of primary interest in this study is the reliability of this method when subjected to variability in the internal parameters of the method (i.e., binning procedures, threshold values, etc.), scatter among individual profiles and the robustness of the linear regression through their mean, and uncertainty in the SST estimate. In addition, a high-resolution large-eddy simulation of an idealized tropical cyclone vortex was used to further validate this procedure by constructing simulated sonde profiles from the simulation and performing an identical retrieval of surface flux coefficients. In this case, the value of SST is known exactly, and the estimated values of C_D and C_K were compared to the prescribed values in the numerical code.

Overall, the results show that estimates of C_D using dropsonde data, as done by Powell et al. (2003) and Holthuijsen et al. (2012), are accurate to within approximately 50% up to wind speeds of roughly 50 m s^{-1}. This includes the sensitivity of this method to regression procedures as well as its ability to quantitatively recover prescribed surface values in the numerical simulations. While a relative error of 50% could be considered somewhat large, it does not preclude one from using the flux profile method estimates of C_D to confirm qualitative conclusions about the behavior of the drag coefficient at high winds.

For computing C_K, on the other hand, this analysis shows that, while the estimated values lie in the same general range as others in the literature (Zhang et al. 2008; Bell et al. 2012; Jeong et al. 2012), variability of the estimated values is relatively high, restricting a quantitative prediction to only within 200%. The uncertainty in SST is a major source of this variability, but inherent sensitivity in the binning procedure leads to large spread as well, limiting the ability of the flux profile method to predict surface flux coefficients even if SST were somehow known. Beyond this, violations of MO theory, particularly near the tropical cyclone eye, potentially corrupt the predictions of both C_D and C_K; likewise, other factors, such as neglecting surface currents in the computation of C_D, may impact the accuracy as well.

The flux profile technique thus provides a means of roughly estimating quantities such as C_D and C_K, however with limited quantitative skill. While it may guide qualitative considerations, such as whether or not the value of C_D saturates (Powell et al. 2003) or whether or not spray influences enthalpy fluxes (Richter and Stern 2014), its use as a tool for refining values of C_D or C_K is not recommended. If one were interested in the surface fluxes themselves (as opposed to the flux coefficients), knowledge of SST and other surface conditions is not required, and predictions via the flux profile method are quite robust (assuming conditions for MO theory hold); however, these quantities are of much less practical use for universal surface flux parameterizations.

Acknowledgments. The authors would like to acknowledge the National Oceanic and Atmospheric Administration's Hurricane Research Division for making the dropsonde data used in this study publicly available. The authors would also like to thank George Bryan for helpful discussions, as well as three reviewers who helped improve the quality of the manuscript.

REFERENCES

Andreas, E. L, 2004: Spray stress revisited. *J. Phys. Oceanogr.*, **34**, 1429–1440, doi:10.1175/1520-0485(2004)034<1429:SSR>2.0.CO;2.

——, 2010: Spray-mediated enthalpy flux to the atmosphere and salt flux to the ocean in high winds. *J. Phys. Oceanogr.*, **40**, 608–619, doi:10.1175/2009JPO4232.1.

——, 2011: Fallacies of the enthalpy transfer coefficient over the ocean in high winds. *J. Atmos. Sci.*, **68**, 1435–1445, doi:10.1175/2011JAS3714.1.

Bao, J.-W., C. W. Fairall, S. A. Michelson, and L. Bianco, 2011: Parameterizations of sea-spray impact on the air–sea momentum and heat fluxes. *Mon. Wea. Rev.*, **139**, 3781–3797, doi:10.1175/MWR-D-11-00007.1.

Bell, M. M., M. T. Montgomery, and K. A. Emanuel, 2012: Air–sea enthalpy and momentum exchange at major hurricane wind speeds observed during CBLAST. *J. Atmos. Sci.*, **69**, 3197–3222, doi:10.1175/JAS-D-11-0276.1.

Bi, X., and Coauthors, 2015: Observed drag coefficients in high winds in the near offshore of the South China Sea. *J. Geophys. Res. Atmos.*, **120**, 6444–6459, doi:10.1002/2015JD023172.

Black, P. G., and Coauthors, 2007: Air–sea exchange in hurricanes: Synthesis of observations from the Coupled Boundary Layer Air–Sea Transfer experiment. *Bull. Amer. Meteor. Soc.*, **88**, 357–374, doi:10.1175/BAMS-88-3-357.

Bryan, G. H., 2012: Effects of surface exchange coefficients and turbulence length scales on the intensity and structure of numerically simulated hurricanes. *Mon. Wea. Rev.*, **140**, 1125–1143, doi:10.1175/MWR-D-11-00231.1.

——, 2013: Comments on sensitivity of tropical-cyclone models to the surface drag coefficient. *Quart. J. Roy. Meteor. Soc.*, **139**, 1957–1960, doi:10.1002/qj.2066.

——, and J. M. Fritsch, 2002: A benchmark simulation for moist nonhydrostatic numerical models. *Mon. Wea. Rev.*, **130**, 2917–2928, doi:10.1175/1520-0493(2002)130<2917:ABSFMN>2.0.CO;2.

——, and R. Rotunno, 2009: The maximum intensity of tropical cyclones in axisymmetric numerical model simulations. *Mon. Wea. Rev.*, **137**, 1770–1789, doi:10.1175/2008MWR2709.1.

——, and H. Morrison, 2012: Sensitivity of a simulated squall line to horizontal resolution and parameterization of

microphysics. *Mon. Wea. Rev.*, **140**, 202–225, doi:10.1175/MWR-D-11-00046.1.

D'Asaro, E. A., and Coauthors, 2013: Impact of typhoons on the ocean in the Pacific. *Bull. Amer. Meteor. Soc.*, **95**, 1405–1418, doi:10.1175/BAMS-D-12-00104.1.

Davis, C., 2015: The formation of moist vortices and tropical cyclones in idealized simulations. *J. Atmos. Sci.*, **72**, 3499–3516, doi:10.1175/JAS-D-15-0027.1.

Deardorff, J. W., 1980: Stratocumulus-capped mixed layers derived from a three-dimensional model. *Bound.-Layer Meteor.*, **18**, 495–527, doi:10.1007/BF00119502.

DeCosmo, J., K. B. Katsaros, S. D. Smith, R. J. Anderson, W. A. Oost, K. Bumke, and H. Chadwick, 1996: Air–sea exchange of water vapor and sensible heat: The Humidity Exchange over the Sea (HEXOS) results. *J. Geophys. Res.*, **101**, 12 001–12 016, doi:10.1029/95JC03796.

Dingman, S. L., 2008: *Physical Hydrology*. 2nd ed. Waveland Press, 646 pp.

Donelan, M. A., B. K. Haus, N. Reul, W. J. Plant, M. Stiassnie, H. C. Graber, O. B. Brown, and E. S. Saltzman, 2004: On the limiting aerodynamic roughness of the ocean in very strong winds. *Geophys. Res. Lett.*, **31**, L18306, doi:10.1029/2004GL019460.

Drennan, W. M., J. A. Zhang, J. R. French, C. McCormick, and P. G. Black, 2007: Turbulent fluxes in the hurricane boundary layer. Part II: Latent heat flux. *J. Atmos. Sci.*, **64**, 1103–1115, doi:10.1175/JAS3889.1.

Dunion, J. P., 2011: Rewriting the climatology of the tropical North Atlantic and Caribbean Sea atmosphere. *J. Climate*, **24**, 893–908, doi:10.1175/2010JCLI3496.1.

Edson, J. B., and Coauthors, 2013: On the exchange of momentum over the open ocean. *J. Phys. Oceanogr.*, **43**, 1589–1610, doi:10.1175/JPO-D-12-0173.1.

Emanuel, K. A., 1986: An air–sea interaction theory for tropical cyclones. Part I: Steady-state maintenance. *J. Atmos. Sci.*, **43**, 585–605, doi:10.1175/1520-0469(1986)043<0585:AASITF>2.0.CO;2.

——, 1995: Sensitivity of tropical cyclones to surface exchange coefficients and a revised steady-state model incorporating eye dynamics. *J. Atmos. Sci.*, **52**, 3969–3976, doi:10.1175/1520-0469(1995)052<3969:SOTCTS>2.0.CO;2.

Fairall, C. W., J. D. Kepert, and G. J. Holland, 1994: The effect of sea spray on surface energy transports over the ocean. *Global Atmos. Ocean Syst.*, **2**, 121–142.

——, E. F. Bradley, J. E. Hare, A. A. Grachev, and J. B. Edson, 2003: Bulk parameterization of air–sea fluxes: Updates and verification for the COARE algorithm. *J. Climate*, **16**, 571–591, doi:10.1175/1520-0442(2003)016<0571:BPOASF>2.0.CO;2.

French, J. R., W. M. Drennan, J. A. Zhang, and P. G. Black, 2007: Turbulent fluxes in the hurricane boundary layer. Part I: Momentum flux. *J. Atmos. Sci.*, **64**, 1089–1102, doi:10.1175/JAS3887.1.

Green, B. W., and F. Zhang, 2013: Impacts of air–sea flux parameterizations on the intensity and structure of tropical cyclones. *Mon. Wea. Rev.*, **141**, 2308–2324, doi:10.1175/MWR-D-12-00274.1.

——, and ——, 2014: Sensitivity of tropical cyclone simulations to parametric uncertainties in air–sea fluxes and implications for parameter estimation. *Mon. Wea. Rev.*, **142**, 2290–2308, doi:10.1175/MWR-D-13-00208.1.

Haus, B. K., D. Jeong, M. A. Donelan, J. A. Zhang, and I. Savelyev, 2010: Relative rates of sea–air heat transfer and frictional drag in very high winds. *Geophys. Res. Lett.*, **37**, L07802, doi:10.1029/2009GL042206.

Hock, T. F., and J. L. Franklin, 1999: The NCAR GPS dropwindsonde. *Bull. Amer. Meteor. Soc.*, **80**, 407–420, doi:10.1175/1520-0477(1999)080<0407:TNGD>2.0.CO;2.

Holthuijsen, L. H., M. D. Powell, and J. D. Pietrzak, 2012: Wind and waves in extreme hurricanes. *J. Geophys. Res.*, **117**, C09003, doi:10.1029/2012JC007983.

Jarosz, E., D. A. Mitchell, D. W. Wang, and W. J. Teague, 2007: Bottom-up determination of air–sea momentum exchange under a major tropical cyclone. *Science*, **315**, 1707–1709, doi:10.1126/science.1136466.

Jeong, D., B. K. Haus, and M. A. Donelan, 2012: Enthalpy transfer across the air–water interface in high winds including spray. *J. Atmos. Sci.*, **69**, 2733–2748, doi:10.1175/JAS-D-11-0260.1.

Kudryavtsev, V. N., and V. K. Makin, 2007: Aerodynamic roughness of the sea surface at high winds. *Bound.-Layer Meteor.*, **125**, 289–303, doi:10.1007/s10546-007-9184-7.

Makin, V. K., 2005: A note on the drag of the sea surface at hurricane winds. *Bound.-Layer Meteor.*, **115**, 169–176, doi:10.1007/s10546-004-3647-x.

Mangarella, P. A., A. J. Chambers, R. L. Street, and E. Y. Hsu, 1973: Laboratory studies of evaporation and energy transfer through a wavy air–water interface. *J. Phys. Oceanogr.*, **3**, 93–101, doi:10.1175/1520-0485(1973)003<0093:LSOEAE>2.0.CO;2.

Monin, A. S., and A. M. Yaglom, 1971: *Statistical Fluid Mechanics*. Vol. 1. Dover Publications, 769 pp.

Montgomery, M. T., R. K. Smith, and S. V. Nguyen, 2010: Sensitivity of tropical-cyclone models to the surface drag coefficient. *Quart. J. Roy. Meteor. Soc.*, **136**, 1945–1953, doi:10.1002/qj.702.

Mueller, J. A., and F. Veron, 2014: Impact of sea spray on air–sea fluxes. Part II: Feedback effects. *J. Phys. Oceanogr.*, **44**, 2835–2853, doi:10.1175/JPO-D-13-0246.1.

Potter, H., H. C. Graber, N. J. Williams, C. O. Collins, R. J. Ramos, and W. M. Drennan, 2015: In situ measurements of momentum fluxes in typhoons. *J. Atmos. Sci.*, **72**, 104–118, doi:10.1175/JAS-D-14-0025.1.

Powell, M. D., P. J. Vickery, and T. A. Reinhold, 2003: Reduced drag coefficient for high wind speeds in tropical cyclones. *Nature*, **422**, 279–283, doi:10.1038/nature01481.

Reichl, B. G., T. Hara, and I. Ginis, 2014: Sea state dependence of the wind stress over the ocean under hurricane winds. *J. Geophys. Res. Oceans*, **119**, 30–51, doi:10.1002/2013JC009289.

Reynolds, R. W., T. M. Smith, C. Liu, D. B. Chelton, K. S. Casey, and M. G. Schlax, 2007: Daily high-resolution-blended analyses for sea surface temperature. *J. Climate*, **20**, 5473–5496, doi:10.1175/2007JCLI1824.1.

Richter, D. H., and D. P. Stern, 2014: Evidence of spray-mediated air–sea enthalpy flux within tropical cyclones. *Geophys. Res. Lett.*, **41**, 2997–3003, doi:10.1002/2014GL059746.

Rios-Berrios, R., T. Vukicevic, and B. Tang, 2014: Adopting model uncertainties for tropical cyclone intensity prediction. *Mon. Wea. Rev.*, **142**, 72–78, doi:10.1175/MWR-D-13-00186.1.

Rosenthal, S. L., 1971: The response of a tropical cyclone model to variations in boundary layer parameters, initial conditions, lateral boundary conditions, and domain size. *Mon. Wea. Rev.*, **99**, 767–777, doi:10.1175/1520-0493(1971)099<0767:TROATC>2.3.CO;2.

Smith, R. K., and M. T. Montgomery, 2014: On the existence of the logarithmic surface layer in the inner core of hurricanes. *Quart. J. Roy. Meteor. Soc.*, **140**, 72–81, doi:10.1002/qj.2121.

Sraj, I., and Coauthors, 2013: Bayesian inference of drag parameters using AXBT data from Typhoon Fanapi. *Mon. Wea. Rev.*, **141**, 2347–2367, doi:10.1175/MWR-D-12-00228.1.

Sullivan, P. P., and J. C. McWilliams, 2010: Dynamics of winds and currents coupled to surface waves. *Annu. Rev. Fluid Mech.*, **42**, 19–42, doi:10.1146/annurev-fluid-121108-145541.

Takagaki, N., S. Komori, N. Suzuki, K. Iwano, T. Kuramoto, S. Shimada, R. Kurose, and K. Takahashi, 2012: Strong correlation between the drag coefficient and the shape of the wind sea spectrum over a broad range of wind speeds. *Geophys. Res. Lett.*, **39**, L23604, doi:10.1029/2012GL053988.

Troitskaya, Y. I., D. A. Sergeev, A. A. Kandaurov, G. A. Baidakov, M. A. Vdovin, and V. I. Kazakov, 2012: Laboratory and theoretical modeling of air–sea momentum transfer under severe wind conditions. *J. Geophys. Res.*, **117**, C00J21, doi:10.1029/2011JC007778.

Veron, F., 2015: Ocean spray. *Annu. Rev. Fluid Mech.*, **47**, 507–538, doi:10.1146/annurev-fluid-010814-014651.

Vickers, D., L. Mahrt, and E. L Andreas, 2013: Estimates of the 10-m neutral sea surface drag coefficient from aircraft eddy-covariance measurements. *J. Phys. Oceanogr.*, **43**, 301–310, doi:10.1175/JPO-D-12-0101.1.

Zhang, J. A., P. G. Black, J. R. French, and W. M. Drennan, 2008: First direct measurements of enthalpy flux in the hurricane boundary layer: The CBLAST results. *Geophys. Res. Lett.*, **35**, L14813, doi:10.1029/2008GL034374.

Zhao, Z.-K., C.-X. Liu, Q. Li, G.-F. Dai, Q.-T. Song, and W.-H. Lv, 2015: Typhoon air–sea drag coefficient in coastal regions. *J. Geophys. Res. Oceans*, **120**, 716–727, doi:10.1002/2014JC010283.